Hindawi
Mobile Information Systems
Volume 2023, Article ID 4006715, 11 pages
https://doi.org/10.1155/2023/4006715

Research Article

Intelligent Testing and Analysis of Dissimilar Steel Welds for Industrial Throttle Flowmeter

Lianghuai Tong[1], **Hui Xu**[2], **Xiaojie Xu**[1], **Huaye Cheng**[1], **Feng Li**[3] and **Jiahui Zhou**[4]

[1]*Quzhou Academy of Metrology and Quality Inspection, Quzhou, China*
[2]*Hangzhou Special Equipment Testing and Research Institute, Hangzhou, China*
[3]*Zhejiang Province Metallurgic Products Quality Test Station Co.,Ltd., Hangzhou, China*
[4]*Zhejiang University, Hangzhou, China*

Correspondence should be addressed to Xiaojie Xu; csccpv@163.com

Received 30 August 2022; Revised 6 October 2022; Accepted 16 April 2023; Published 25 May 2023

Academic Editor: Wang Wenyong

The throttling flowmeter used in utility boilers has been used as a measuring instrument for a long time. However, its safety performance, such as welding, lacks enough attention. The manufacturing welds of the throttling flowmeter are welded with austenitic stainless steel and pearlitic heat-resistant steel. Cracks and other defects are generally found in the inspection and detection of the manufacturing welds of throttling flowmeters in service, which have serious potential accidents. To find out the relationship between weldingdissimilar steels and defects, the microhardness indentation method was used to measure the residual stress of welding. Combined with the self-developed calculation software of microscopic indentation residual stress distribution, we used the difference between the color of the indentation area and the surrounding area to quickly measure the indentation strain collected by the microscope using the computer image recognition algorithm, which greatly improved the accuracy and speed of the microscopic indentation residual stress test. The results show that the residual stress at the weld of dissimilar steel is relatively large, and the mechanical property test is generally unqualified. The microindentation residual stress analysis method based on computer image recognition is used to quickly, intuitively, and accurately reveal the direct relationship between the combination of dissimilar steel welding materials and the generation of cracks and other defects.

1. Introduction

The throttling flowmeter used in utility boilers is ubiquitous and is applied in high-temperature and high-pressure environments. The welding seam is generally welded between austenitic stainless steel and pearlitic heat-resistant dissimilar steel. The quality of the welding seam is very important, which is related to whether the throttling flowmeter can be used safely. Many scholars have carried out research on the welding problems of austenitic stainless steel and pearlitic heat-resistant dissimilar steel and the detection and analysis methods of welding defects.

Defects in the form of pores and slag inclusions usually appear in the welds of austenitic stainless steel and pearlitic heat-resistant dissimilar steel, thus causing local strain concentration. In austenitic steel and pearlitic steel, pores of 1 to 3 mm and slag inclusion will reduce the thermal fatigue life of welded joints by more than 10 times [1]. Scanning electron microscopy, transmission electron microscopy, and energy dispersive X-ray spectroscopy adopted by Gotalskii et al. [2] directly observed the weld interface of austenitic steel and pearlitic steel dissimilar alloy welds, and they found that there are two types of interfaces: austenite/martensite and martensite-like/ferrite. Pan and Zhang [3] proposed a method to reduce the width of such martensite interfaces. Schmidova et al. [4] performed hardness measurements in critical areas of pearlitic and austenitic steel welds and translated them into carbon concentration changes, which confirmed the presence of large concentrations and structural inhomogeneity at the fusion line, and such fusion zones

were considered to be unstable [5]. Li et al. [6] and Nelson et al. [7] also analyzed the fusion zone and found it to be characterized by chemical inhomogeneity between the weld and the base metal. Danielewski et al. [8] conducted metallographic analysis of the weld and found that in stainless steel, the heat-affected zone was very narrow, and the growth of austenite grains was not observed, while the slender grains of ferrite formed a discontinuous network around the austenite grain. Another problem with dissimilar steel welds between austenitic steel and pearlitic steel is the presence of decarburization and carbide interlayers, which have an adverse effect on the mechanical properties of the welding seam [9]. Nikulina et al. [10] studied the flash butt welding of high-carbon pearlitic steel and chromium-nickel austenitic steel, and the results showed that layered pearlite colonies containing chromium and nickel and thin austenite interlayers were formed in the weld zone. Vishniakas [11] found that the failure of austenitic electrode welds was viscous, and individual parts were quasibrittle failures, while the failures of ferritic and pearlitic electrode welds were moderate. Elagin et al. [12] found that during long-term high-temperature heating, the formation of nitride particles and grain refinement help to improve the microstructure stability of the weld, inhibit the development of carbide reactions, and reduce the microstructure inhomogeneity of the weld. Therefore, the carbides are distributed more uniformly in the fusion zone with pearlitic steel, thereby reducing the hot brittleness of dissimilar steel welds. Li and Yan [13] used plasma arc welding to weld dissimilar steels of pearlitic steel and austenitic steel and also found that a plate-like martensitic hardened layer was formed in the welding zone, carbon migrated on both sides of the welded joint, and there was a central area of lower hardness. Chu et al. [14] analyzed the failure causes of a certain weld and found that there were intergranular holes and cracks around the main crack, and the main failure mechanism was creep cracking. Dupont [15] summarized the welding of dissimilar steels, where premature failure is usually caused by the following factors: abrupt changes in the microstructure and mechanical properties at the fusion line; large differences in coefficient of thermal expansion (CTE) between ferritic and austenitic alloys; the formation of interfacial carbides, which leads to the formation of creep voids; and the preferential oxidation of ferritic steels near the fusion line.

For the inspection of welds, some standards and manuals have been issued for reference [16, 17]. In addition, except for some traditional inspection methods, new inspection methods are also emerging. Thuvander et al. [18] combined magnetic force microscopy (MFM) with scanning electron microscopy to successfully study austenitic and duplex stainless steel weld metals with different ferrite levels. Hempel [19] conducted an in-depth study on the residual stress state of dissimilar steel welds using X-ray and neutron diffraction and confirmed that the residual stress on the surface of austenitic tubes during sample preparation was greatly affected by the machining technology. Barat et al. [9] experimentally confirmed that the acoustic emission method can be used to detect both typical welding defects in welded joints of different structural grades of steel as well as diffusion interlayers. Lyubimova et al. [20] proposed that the combination of X-ray fluorescence analysis, X-ray diffraction, and microhardness determination with traditional inspection methods (visual or ultrasonic inspection [21], etc.) can improve the operational reliability of dissimilar steel welds. Finite element analysis of welding deformation and residual stress was performed by Bouchard [22] and Rong et al. [23], which can be used to predict the transient behavior of welding deformation and residual stress. Woo et al. [24] and Eisazadeh et al. [25] used the neutron diffraction method to measure the residual stress of different welding layer thicknesses and different welds. The transverse residual stress caused by welding was related to the existence of the martensite phase in dissimilar welds. Rathod et al. [26] concluded that radiography techniques could not detect small inclusions in welds. Therefore, the quality of detection should be checked by additional NDT detection such as ultrasound [27]. Ultrasonic testing requires materials that are acoustically isotropic, whereas austenitic welding materials are highly anisotropic due to the dendritic structure created by the cooling process during welding. Bulavinov [28] addressed this issue with an in-depth understanding of sound propagation in welded structures through elastodynamic simulations to support the assessment of the local structure of the weld. Juengert [29] developed two ultrasonic inspection techniques and validated them on planar specimens with artificial and real defects; both reconstruction techniques gave quantitative inspection results and allowed the determination of defect sizes. Lugin [30] proposed a new method to detect hidden defects using lateral heat flow, which can find hidden defects/cracks that cannot be detected by traditional thermal detection methods. It is a common method to collect welding stress data using Internet of Things technology [31, 32].

Xia et al. [33] developed a method based on microindentation, which could predict the length of the crack as a function of the residual thermal stresses. Mulford et al. [34] described a procedure for extracting simple constitutive parameters from microindentation tests to construct the entire stress versus strain curve. Frutos et al. [35] addressed the determination of residual stresses in sandblasted austenitic steel by ultramicroindentation techniques using a sharp indenter. The results showed good agreement with those obtained by synchrotron radiation on the same specimens. Yonezu et al. [36] proposed a method to evaluate the residual stress and plastic strain of an austenitic stainless steel using a microindentation test. A numerical experiment with the finite element method (FEM) was carried out to simulate an indentation test for SUS316L with various plastic strains (prestrains) and residual stresses. Liu et al. [37] investigated the microstructure and residual stress of laser rapid formed (LRFed) nickel-base superalloy Inconel 718, and residual stress evaluation in microstructure scale by Vickers microindentation method indicates that the residual thermal stress is unevenly distributed in the LRFed sample.

Although dissimilar steel welding of austenitic stainless steel and pearlitic heat-resistant steel is widely used in utility boiler pipes, and domestic and foreign research studies have also been carried out on the problems of dissimilar steel

welding and the detection and analysis methods of welding defects, less research has been done on the welding of dissimilar steels on the throttling flowmeter. For a long time, the throttling flowmeter was only used as a measuring instrument, and its safety performance, such as welding, lacked attention. It was not until 2016 that the explosion of the flowmeter of the Dangyang Power Plant in Hubei caused serious casualties, and all parties in the society began to pay attention to its safety. In this paper, the standard nozzle flowmeter (hereinafter referred to as the nozzle flowmeter) in the throttling flowmeter is taken as the research object, the structure and process of the welding seam of the throttling flowmeter are simulated, and different combinations of dissimilar steel welding materials are selected to make the processing test pieces. Then, the microhardness method combined with the microindentation residual stress distribution calculation software was used to test the residual stress and mechanical properties of the weld of the specimen. The relationship between welding of dissimilar steels and defects is analyzed, and the reasons why throttling flowmeters are pervasive in deficiencies are revealed, which provides a direction for the next step of the flowmeter's structural transformation and processing technology improvement.

2. Problems Existing in the Welding Seam of Throttling Flowmeter

The throttling flowmeters used in utility boilers are similar in structure. The example used in this case is the standard nozzle flowmeter, also known as the nozzle flowmeter, as shown in Figure 1. In order to ensure strength as a pressure-bearing part in a high temperature and high pressure environment, the front and rear clamping rings are generally made of pearlitic heat-resistant steel. To ensure the geometric size of the throttling part and guarantee the measurement accuracy as a measuring element as well as maintain the cleanliness of the surface and prevent oxidation at high temperature, the throttling parts are generally made of austenitic stainless steel. Due to the inconsistent materials of the front and rear clamping rings and the throttling parts, the welding seam has a problem of dissimilar steel welding. To be specific, the welding of austenitic stainless steel and pearlitic heat-resistant steel, and the welding seam is V-shaped.

The author collected 9 out of 53 nozzle flowmeters from 8 thermal power companies in a targeted manner, involving 4 user units and 5 manufacturing units, also taking into account the different materials, operating parameters, different media, and operating times of the nozzle flowmeter. After taking advantage of the convenient conditions of the laboratory, by means of dissection, nondestructive testing, scanning electron microscope, energy spectrum analysis, mechanical performance tests, etc., it was found that none of the nozzle flowmeters survived. To be specific, cracks and other associated defects were found in the manufacturing welds of the nozzle flowmeters that were sampled, as shown in Figures 2–5. The defect rate is 100%, and the high incidence of flowmeters is shocking.

3. The Basic Situation of Welding Specimens of Throttling Flowmeter

To verify the relationship between the welding of dissimilar steel for the throttling flowmeter of a utility boiler and the defects such as cracks commonly found on the weld, the structure and process of the welding seam of the throttling flowmeter were simulated, and different combinations of dissimilar steel welding consumables were selected to make processing test pieces. Then, the residual stress and mechanical properties of the welds of the specimens were tested by appropriate test methods. The structure and welding process of the throttling flowmeter weld were simulated, and different combinations of dissimilar steel welding consumables were selected, including process test pieces 1 to 4 (see Figures 6–9). The hardness and welding residual stress of the specimens under different welding processes were analyzed, and the mechanical properties of the specimens were also tested; the results are shown in Table 1.

4. Selection of Residual Stress Test Method

The traditional measurement techniques of residual stress of welded components can be roughly divided into two categories: the mechanical release measurement method with certain damage and the nondestructive physical measurement method. These measurement methods are basically only macroscopic measurement methods, which means the test process is difficult to repeat and the experimental data are widely distributed. In addition, mechanical methods, such as the blind hole method will cause greater damage to the measurement samples. In recent 10 years, due to the development of thin film materials and nanotechnology, traditional measurement methods have been unable to meet the experimental requirements, and a new residual stress measurement technology has emerged: the use of microhardness indentation to measure residual stress.

The basic measurement principle of residual stress measured by the microhardness indentation method is that there is a linear relationship between residual stress (strain) and indentation area ratio. When there is tensile stress in the sample, depressions will occur around the indentation, and the area of the indentation will be relatively small. When there is compressive stress, there will be bulges around the indentation, and the area of the indentation will be relatively large. That is why the hardness method for measuring the residual stress of the material is determined by the ratio of the indentation area on the surface of the sample.

According to the theory of OliverWC and PharrGM, the residual stress is sensitive to the amount of metal accumulated around the indentation during the pressing process, so the primary condition for accurate residual stress measurement is to accurately measure the area change of the indentation. The introduction of the parameter indentation area ratio C^2 is given below:

$$c^2 = \frac{A}{A_{\text{nom}}}. \tag{1}$$

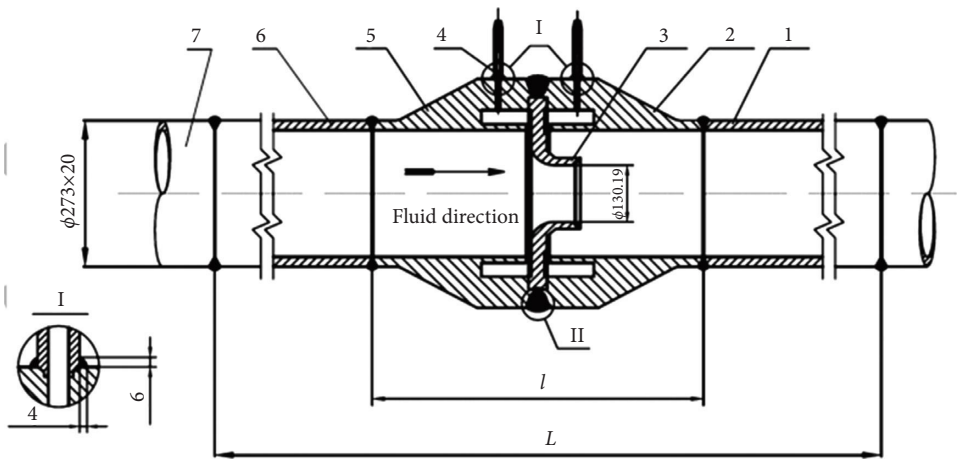

1,6-Measuring tube, 2-Rear clamping ring, 3-Nozzle, 4-Pressure tube,
5-Front clamping ring, 7-Process piping

Figure 1: Assembly drawing of $\Phi 273 \times 25$ mm standard nozzle flowmeter.

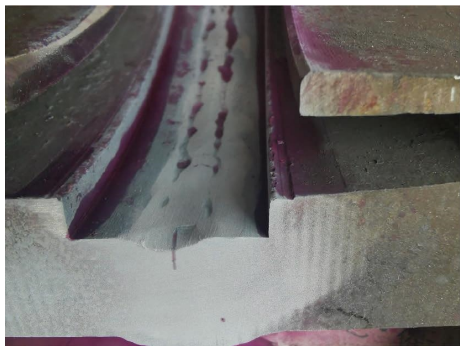

Figure 2: Crack at the root of the weld seam of throttling flowmeter.

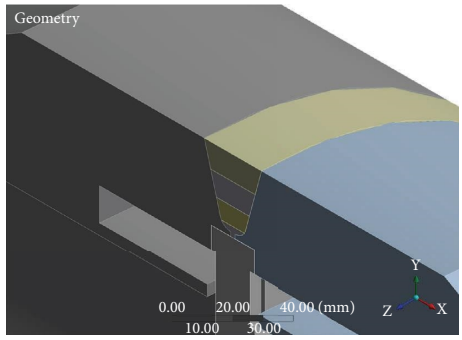

Figure 3: Weld structure diagram of throttling flowmeter.

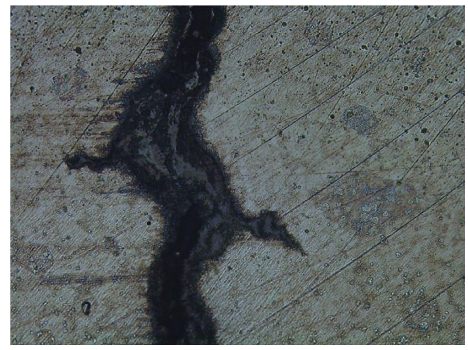

Figure 4: Metallographic diagram of the first layer crack of weld (200 times).

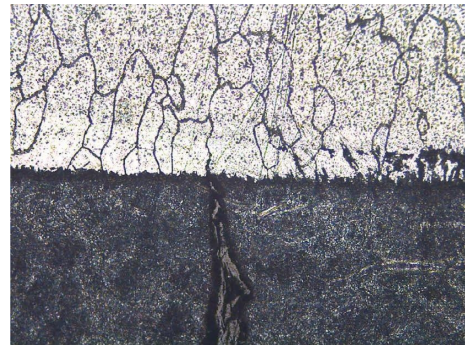

Figure 5: Metallographic diagram of cracks at the junction of the first layer and the second layer of weld seams.

A_{nom} is the projected area of indentation under stress state; A is the area under stress-free state.

The residual stress is finally obtained by calculating the residual strain due to the area change caused by the residual stress.

However, the microhardness indentation method also has some limitations. For example, in order to test the residual stress on the cross section of the weld, it is necessary to take a sample of the weld section, which destroys the integrity of the weld inevitably and only the residual stress in the two-dimensional direction of the cutting plane can be measured, which means the actual residual stress at the test point cannot be completely reflected. Due to the irregularity of the indentation shape affected by residual stress, the accuracy and time-consuming nature of traditional dimensional measurement methods limit the application of this test method in practical engineering. In addition, the

Figure 6: 1# pipe sample.

Figure 7: 2# pipe sample.

Figure 8: 3# pipe sample.

Figure 9: 4# pipe sample.

Table 1: Welding specimen.

No.	Shell material	Shell thickness (mm)	Throttling material	Bottom welding material	Cover welding material	Heat treatment
Specimen 1	12Cr1MoVG	28	304	R31	R317	Yes
Specimen 2	12Cr1MoVG	28	304	ER308	R317	No
Specimen 3	12Cr1MoVG	28	304	ER309	R317	No
Specimen 4	12Cr1MoVG	28	304	ER309	R317	Yes

residual stress is calculated through the relationship between the residual stress and the residual strain. The residual stress between adjacent test points sometimes has a large difference, with peak values and some discontinuities.

To find out the distribution rules of welding residual stress on the welding seam cross section of the throttling flowmeter, the microhardness indentation method was used in this welding residual stress test. The author used the self-developed "microindentation residual stress distribution calculation software" and utilized the difference between the color of the indentation area and the surrounding area. The flow of the algorithm is shown in Figure 10. The computer image recognition algorithm was used to quickly measure the indentation strain collected by the microscope, which greatly improved the testing accuracy and speed of residual stress by microindentation. The software functions included image recognition of indentation topography, automatic calculation of actual area of indentation, theoretical area of indentation, residual strain, and residual stress. It can perform one-click batch identification and calculation of indentation photos.

The key to improving the accuracy and speed of microindentation measurement lies in the rapid and accurate determination of the indentation area of complex shapes that are actually deformed by residual stress. The traditional microscope cannot measure the size and calculate the area of the actual indentation with concave-convex arc features. Using the light and shade difference between the indentation and the surrounding material in the metallographic photo, the computer image recognition method is used to directly extract the sum of the pixels of the dark indentation as the actual indentation area, and the diagonal pixel length between the four endpoints is extracted to obtain the theoretical Indentation area. The ratio of the two can cancel the influence of the pixel unit and the length unit and avoid the difficulty of the actual indentation size measurement and area calculation.

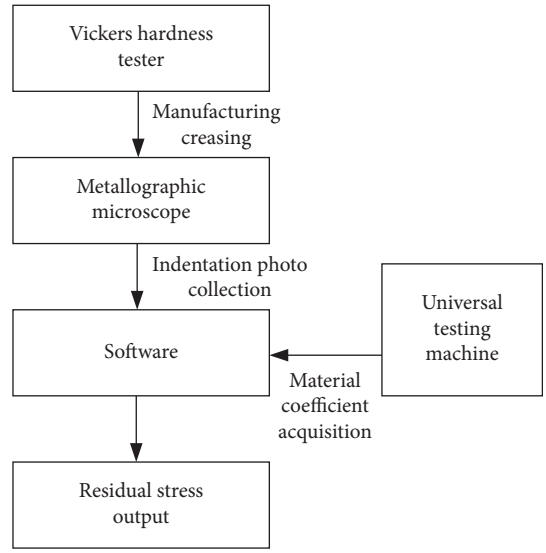

Figure 10: Microindentation residual stress based on computer image recognition algorithm.

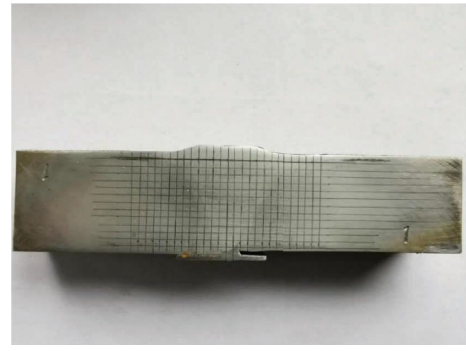

Figure 11: 1#-1 sample.

5. Measurement of Welding Residual Stress on Welding Specimens of Throttling Flowmeter

Weld seam section samples were taken from samples 1#, 2#, 3#, and 4#, respectively, and the samples taken to avoid the arc starting point were recorded as 1#-1, 2#-1, 3#-1, and 4#-1. They were lightly corroded, respectively, and weld distribution can be seen. On the 1#-1 sample, a test point was taken every 2 mm, and a total of 27 columns and 13 rows were taken, totaling 351 points (Figure 11). The microhardness indentation method was used for stress testing, and the microindentation residual stress distribution calculation software was used too. The schematic diagram of the stress distribution is shown in Figure 12. The minimum stress is 97 MPa, and the maximum stress is 291 MPa. On the 2#-1 sample, a test point was taken every 2 mm, with a total of 23 columns and 13 rows, for a total of 299 points (Figure 13. The schematic diagram of stress distribution is shown in Figure 12; the minimum stress is 106 MPa, and the maximum stress is 386 MPa. On the 3#-1 sample, a test point was taken every 2 mm, with a total of 23 columns and 13 rows, for a total of 299 points (Figure 14. The stress distribution diagram is shown in Figure 12. The minimum stress is 122 MPa, and the maximum stress is 398 MPa. On the 4#-1 sample, a test point was taken every 2 mm, with a total of 21

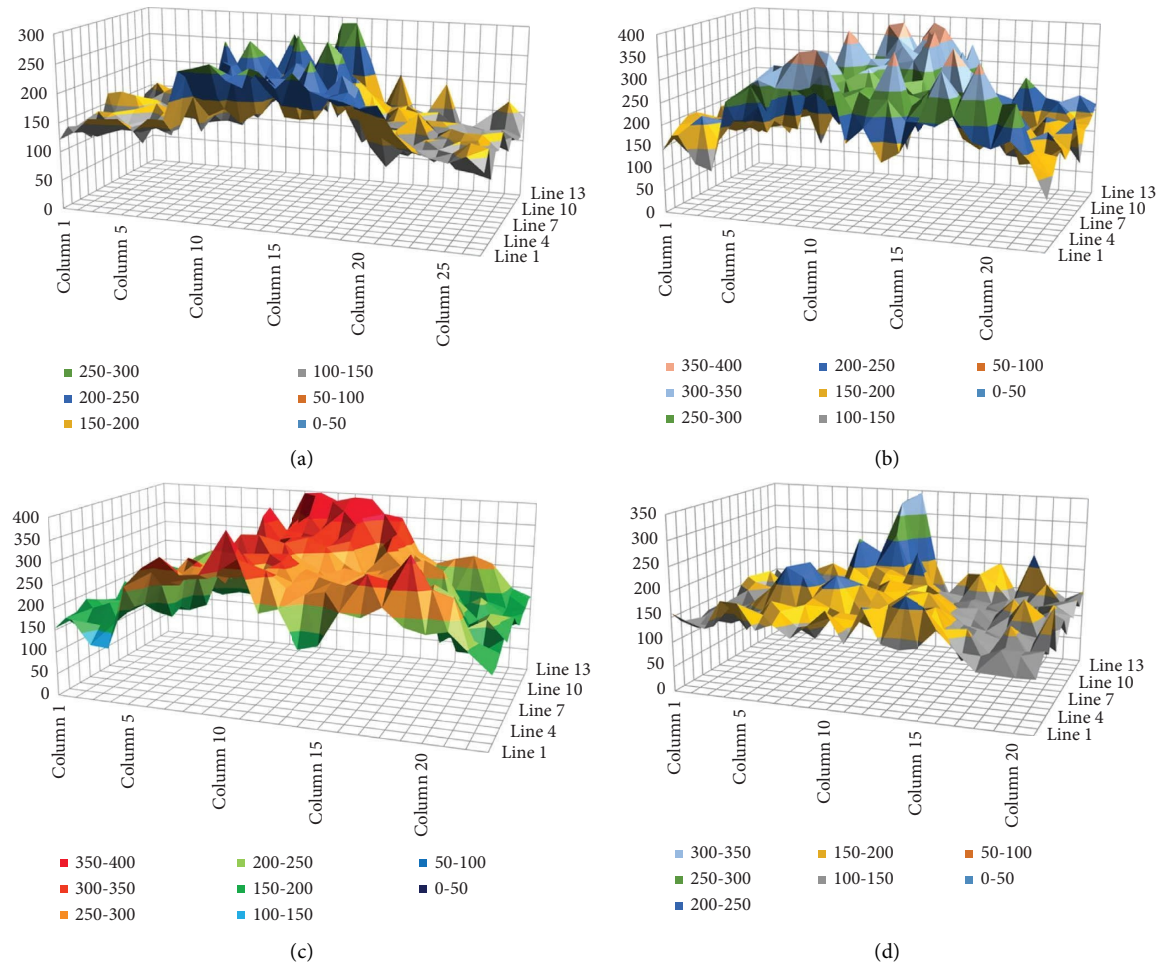

Figure 12: Schematic diagram of stress distribution: (a) sample 1#-1, (b) sample 2#-1, (c) sample 3#-1, and (d) sample 4#-1.

columns and 14 rows, totaling 294 points (Figure 15. The stress distribution diagram is shown in Figure 12. The minimum stress is 102 MPa, and the maximum stress is 346 MPa.

6. Mechanical Properties Test of Welding Specimens of Throttling Flowmeter

According to the requirements of GB/T 228.1-2010, GB/T 2653-2008, and GB/T 229-2007, the mechanical properties of the welds of the four specimens were tested. The test results are shown in Tables 2–4.

7. Analysis of Test Results of Welding Specimens of Throttling Flowmeter

Welding residual stress and mechanical properties test situations are given below:

(1) The welding material of specimen 1 is heat-resistant steel as the base and heat-resistant steel welding rod cover. Except for the welding of dissimilar steel at the welding place between the bottom layer and the stainless steel throttling piece, other welding materials are of the same type. The mechanical properties test reflects that the tensile strength of the welded joint is 539 MPa. The tensile test and impact test results of the welded joint meet the requirements of the specification. However, cracks appeared in some bending specimens of the bottom weld fusion line position of the bending test. The welding residual stress of the specimen is larger than that of the base metal. Most of the residual stress of the weld is between 150 and 250 MPa, and a small part of the point stress is between 250 and 300 MPa. The closer the weld is to the bottom, the greater the welding stress, which is close to 60% of the tensile strength, and there is a certain risk of cracking.

(2) The welding material of specimen 2 is heat-resistant steel and stainless steel transition welding wire as the base and the heat-resistant steel welding rod cover. Due to the transition of welding wire, the heat-resistant steel welding rod will not be in contact with the stainless steel throttling parts. The mechanical performance test reflects that the tensile strength of the welded joint is 500 MPa, and the results of the tensile test, bending test, and the impact

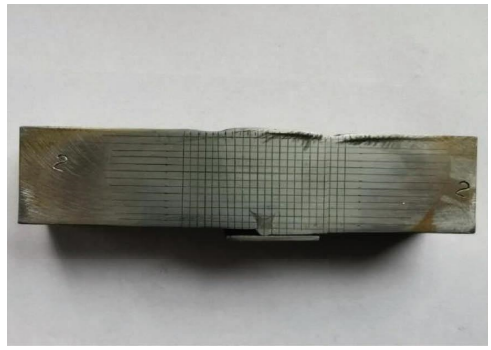

Figure 13: 2#-1 sample.

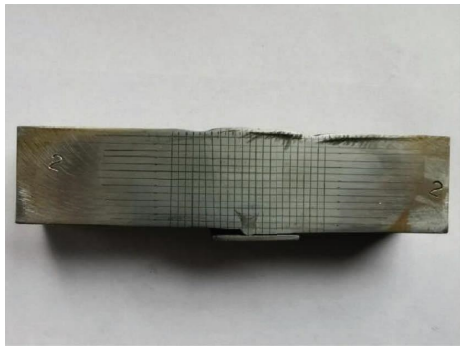

Figure 14: 3#-1 sample.

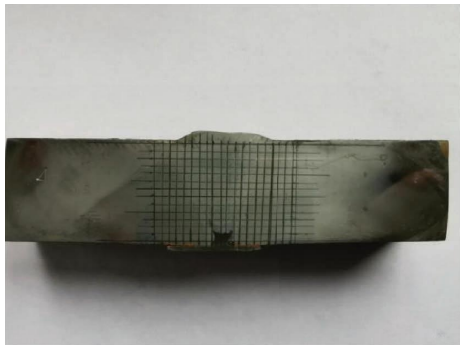

Figure 15: 4#-1 sample.

test of the welded joint all meet the requirements of the specification. The welding residual stress of the specimen is larger than that of the base metal. Since there was no heat treatment performed, most of the residual stress of the weld is between 250 and 350 MPa, and a small part of the point stress is between 350 and 400 MPa. The closer the weld is to the bottom, the greater the welding stress, which is close to 80% of the tensile strength, and there is a greater risk of cracking.

(3) The welding material of specimen 3 is the stainless steel wire as the base and the heat-resistant steel welding rod cover. There is a problem of direct welding of dissimilar steel between the stainless steel wire and the heat-resistant steel welding rod. The mechanical performance test reflects that the tensile strength of the welded joint is 500 MPa, and the tensile test of the welded joint meets the requirements, while the bending test and impact test do not meet the specification requirements. The welding residual stress of the specimen is larger than that of the base metal. Since no heat treatment is performed, most of the residual stress of the weld is between 250 and 350 MPa, and a small part of the point stress is between 350 and 400 MPa. The closer the weld is to the bottom, the greater the welding stress, which is close to 80% of the tensile strength, and there is a great risk of cracking.

Table 2: Tensile test of welded joints of specimens.

No.	Tensile test of welded joint			
	Tensile strength (MPa)		Fracture location	
Specimen 1	539	539	Broken base metal	Broken base metal
Specimen 2	503	498	Broken base metal	Broken base metal
Specimen 3	503	498	Broken base metal	Broken base metal
Specimen 4	503	498	Broken base metal	Broken base metal

(4) The welding material of specimen 4 is the stainless steel wire as the base and the heat-resistant steel welding rod cover. There is a problem of direct welding of dissimilar steel between the stainless steel wire and the heat-resistant steel welding rod. The mechanical performance test reflects that the tensile strength of the welded joint is 500 MPa, and the tensile test of the welded joint meets the requirements, while the bending test and impact test do not meet the specification requirements, but the impact test result is higher than that of specimen 3. The welding residual stress of the specimen is greater than that of the base metal, and the specimen has been heat treated. Most of the residual stress of the weld is between 150 and 250 MPa, and a small part of the point stress is between 250 and 300 MPa. The closer the weld is to the bottom, the greater the welding stress, which is close to 60% of the tensile strength, and there is a certain risk of cracking.

Table 3: Specimen bending test.

No.	Bending test side bend $D = 40$ mm, $\alpha = 180^{\circ}$			
	−1	−2	−3	−4
Specimen 1	No opening defect was found on the curved outer surface	A 1.6 mm long crack on the fusion line	A 3.1 mm long crack on the fusion line	Cracks with lengths of 1.5 mm, 2.8 mm, and 1.7 mm on the fusion line
Specimen 2	No opening defect was found on the curved outer surface	No opening defect was found on the curved outer surface	No opening defect was found on the curved outer surface	No opening defect was found on the curved outer surface
Specimen 3	No opening defect was found on the curved outer surface	A 9.3 mm long crack on the fusion line	A 8.1 mm long crack on the fusion line	Cracks with lengths of 2.3 mm, 4.0 mm and 1.0 mm on the fusion line
Specimen 4	No opening defect was found on the curved outer surface	A 9.3 mm long crack on the fusion line	A 8.1 mm long crack on the fusion line	Cracks with lengths of 2.3 mm, 4.0 mm and 1.0 mm on the fusion line

Table 4: Specimen impact test.

No.	Impact test									
	Weld joint 20°C KV2						Heat affected zone 20°C KV2			
Specimen 1	64	35	43	44	67	183	Unbroken	Unbroken	Unbroken	Unbroken
Specimen 2	84	85	66	77	141	233	183	209	223	221
Specimen 3	11	13	14	26	17	157	183	164	189	153
Specimen 4	18	21	35	23	32	197	204	208	187	175

8. Conclusion

Through the testing of welding residual stress and mechanical properties of specimens with four different welding methods, the test results are comprehensively analyzed below:

(1) There are differences in residual stress between the weld passes of the flowmeter welding specimen. The residual stress near the bottom of the weld is larger, and the residual stress near the end of the weld is smaller. The maximum residual stress is located at the root of the weld, and the local strength is close to 60–80% of the tensile strength of the material, indicating that there is a risk.

(2) If the stainless steel throttling parts are directly welded with heat-resistant steel welding materials or stainless steel welding material base and heat-resistant steel welding material cover, the mechanical properties tests are generally unqualified, and the residual stress at the joint of dissimilar steel is large, indicating that this welding process should be avoided.

(3) The stress of the welded seam of the specimen after heat treatment is obviously lower than that of the welded seam without heat treatment, and the test results of mechanical properties are also better than those of the specimen without heat treatment, indicating that the post-weld heat treatment process can effectively improve the performance of the flowmeter and can be popularized and applied.

Data Availability

The data that support the findings of this study are available from the corresponding author upon reasonable request.

Conflicts of Interest

The authors declare that they have no conflicts of interest.

Acknowledgments

This work was supported in part by the Quzhou City Science and Technology Project under grant nos. 2022K162, 2021K19.

References

[1] A. F. Malygin, "Thermal cyclic strength of welded joints in an austenitic and a pearlitic steel with weld defects," *Welding Production*, vol. 25, no. 8, pp. 25–30, 1978.

[2] Y. U. N. Gotalskii, V. V. Snisar, and D. P. Novikova, "Methods of reducing the width of the martensite interlayer in the fusion zone of a pearlitic steel with an austenitic weld," *Welding Production*, vol. 28, no. 6, pp. 3–5, 1981.

[3] C. Pan and Z. Zhang, "Characteristics of the weld interface in dissimilar austentic-pearlitic steel welds," *Materials Characterization*, vol. 33, no. 2, pp. 87–92, 1994.

[4] E. Schmidova, L. Benes, and K. Stransky, "Structural stability of austenitic surfacing welds of rail profiles part II (experiment)," *Kovove Materialy-Metallic Materials*, vol. 40, no. 2, pp. 113–123, 2002.

[5] Y. Gotalsky, *Welding of Dissimilar Steels*, Kiev, Tekhnika, 1981.

[6] Y. Li, Z. Zou, and B. Zhou, "Microstructure in the weld metal of austenitic-pearlitic dissimilar steels and diffusion of element in the fusion zone," *Journal of Materials Science & Technology*, vol. 17, no. 3, pp. 338–342, 2001.

[7] T. W. Nelson, J. C. Lippold, and M. J. Mills, "Nature and evolution of the fusion boundary in ferritic-austenitic dissimilar weld metals, Part 1 - nucleation and growth," *Welding Journal*, vol. 78, no. 10, pp. 329–s, 1999.

[8] H. Danielewski, A. Skrzypczyk, M. Hebda et al., "Numerical and metallurgical analysis of laser welded, sealed lap joints of s355j2 and 316l steels under different configurations," *Materials*, vol. 13, no. 24, pp. 5819–5822, 2020.

[9] V. Barat, A. Marchenkov, V. Bardakov, M. Karpova, D. Zhgut, and S. Elizarov, "Features of acoustic emission in tensile testing of dissimilar welded joints of pearlitic and austenitic steels," *Applied Sciences*, vol. 11, no. 24, Article ID 11892, 2021.

[10] A. A. Nikulina, A. I. Smirnov, I. A. Bataev, A. A. Bataev, and A. I. Popelyukh, "Growth of lamellar pearlite in the weld zone between dissimilar steels," *The Physics of Metals and Metallography*, vol. 117, no. 1, pp. 54–60, 2016.

[11] I. Vishniakas, "Special features of breaking the welded connections of the ferritic steels," *Mechanika (Kaunas, Lithuania*, vol. 71, no. 3, pp. 66–71, 1995.

[12] V. P. Elagin, V. Lipodaev, and G. Gordan, "Peculiarities of development of structural heterogeneity in the fusion zone of pearlite steel with austenitic nitrogen-containing weld metal," *Paton Welding Journal*, vol. 2016, no. 8, pp. 23–28, 2016.

[13] M. A. Li and Y. Yan, "Microstructure of welded joint of 1Cr17Mn6Ni5N/Q235 dissimilar steel," *Hot Working Technology*, vol. 40, pp. 168–167, 2011.

[14] Q. Chu, M. Zhang, J. Li, Y. Chen, H. Luo, and Q. Wang, "Failure analysis of a steam pipe weld used in power generation plant," *Engineering Failure Analysis*, vol. 44, pp. 363–370, 2014.

[15] J. N. Dupont, "Review of dissimilar metal welding for the NGNP helical-coil steam generator," 2010.

[16] E. V. Deutsches Institut Fur Normung, *Non-destructive Testing of Welds - Visual Testing of Fusion-Welded Joints*, 2017.

[17] P. O. Moore, *Radiographic Testing in Nondestructive Testing Handbook*, American Society for NDT, Columbus, OH, USA, 3 edition, 2005.

[18] M. Thuvander, L. Karlsson, and O. Kazakova, *Magnetic Force Microscopy as a Tool for Weld Metal Studies*, 2002.

[19] N. Hempel, "Residual stress analysis in girth-welded ferritic and austenitic steel pipes using neutron and X-ray diffraction," *Residual Stress: Icrs*, 2017.

[20] L. L. Lyubimova, R. N. Fisenko, R. B. Tabakaev, A. A. Tashlykov, and A. S. Zavorin, "X-ray investigation of a heterogeneous steel weld," *Materials Science and Engineering A*, vol. 682, pp. 248–254, 2017.

[21] E. M. El-Banna, M. S. Nageda, and M. M. Abo El-Saadat, "Study of restoration by welding of pearlitic ductile cast iron," *Materials Letters*, vol. 42, no. 5, pp. 311–320, 2000.

[22] P. J. Bouchard, "Validated residual stress profiles for fracture assessments of stainless steel pipe girth welds," *International Journal of Pressure Vessels and Piping*, vol. 84, no. 4, pp. 195–222, 2007.

[23] Y. Rong, J. Xu, Y. Huang, and G. Zhang, "Review on finite element analysis of welding deformation and residual stress," *Science and Technology of Welding & Joining*, vol. 23, no. 3, pp. 198–208, 2018.

[24] W. Woo, V. Em, C. R. Hubbard, H. J. Lee, and K. S. Park, "Residual stress determination in a dissimilar weld overlay pipe by neutron diffraction," *Materials Science and Engineering A*, vol. 528, no. 27, pp. 8021–8027, 2011.

[25] H. Eisazadeh et al., "A residual stress study in similar and dissimilar welds," *Welding Journal*, vol. 95, no. 4, pp. 111–119, 2016.

[26] D. W. Rathod, S. Pandey, P. Singh, and R. Prasad, "Experimental analysis of dissimilar metal weld joint: ferritic to austenitic stainless steel," *Materials Science and Engineering A*, vol. 639, pp. 259–268, 2015.

[27] Y. M. Gofman, "Estimation of the reliability of testing welded joints of steam pipelines of thermal power plants," *Russian Journal of Nondestructive Testing*, vol. 39, no. 3, pp. 230-231, 2003.

[28] A. Bulavinov, "Ultrasonic inspection of austenitic and dissimilar welds," *E Journal of Nondestructive Testing*.

[29] A. Juengert, "Advanced ultrasonic techniques for nondestructive testing of austenitic and dissimilar welds in nuclear facilities," *44TH ANNUAL REVIEW OF PROGRESS IN QUANTITATIVE NONDESTRUCTIVE EVALUATION*, vol. 37, 2018.

[30] S. Lugin, "Detection of hidden defects by lateral thermal flows," *NDT & E International*, vol. 56, pp. 48–55, 2013.

[31] T. Wang, J. Li, W. Wei, W. Wang, and K. Fang, "Deep learning-based weak electromagnetic intrusion detection method for the zero touch industrial Internet of Things," *IEEE Network*, 2022.

[32] K. Fang, T. Wang, X. Yuan, C. Miao, Y. Pan, and J. Li, "Detection of weak electromagnetic interference attacks based on fingerprint in IIoT systems," *Future Generation Computer Systems*, vol. 126, pp. 295–304, 2022.

[33] Z. Xia, W. A. Curtin, and B. Sheldon, "A new method to evaluate the fracture toughness of thin films," *Acta Materialia*, vol. 52, no. 12, pp. 3507–3517, 2004.

[34] R. Mulford, R. J. Asaro, and R. J. Sebring, "Spherical indentation of ductile power law materials," *Journal of Materials Research*, vol. 19, no. 9, pp. 2641–2649, 2004.

[35] E. Frutos, M. Multigner, and J. L. González-Carrasco, "Novel approaches to determining residual stresses by ultra-microindentation techniques: application to sandblasted austenitic stainless steel," *Acta Materialia*, vol. 58, no. 12, pp. 4191–4198, 2010.

[36] A. Yonezu, R. Kusano, T. Hiyoshi, and X. Chen, "A method to estimate residual stress in austenitic stainless steel using a microindentation test," *Journal of Materials Engineering and Performance*, vol. 24, no. 1, pp. 362–372, 2015.

[37] F. Liu, X. Lin, G. Yang, M. Song, J. Chen, and W. Huang, "Microstructure and residual stress of laser rapid formed Inconel 718 nickel-base superalloy," *Optics & Laser Technology*, vol. 43, no. 1, pp. 208–213, 2011.